CrossMark

ORIGINAL ARTICLE

A three-dimensional digital atlas of the starling brain

Geert De Groof · Isabelle George · Sara Touj · Martin Stacho ·
Elisabeth Jonckers · Hugo Cousillas · Martine Hausberger ·
Onur Güntürkün · Annemie Van der Linden

Abstract Because of their sophisticated vocal behaviour, their social nature, their high plasticity and their robustness, starlings have become an important model species that is widely used in studies of neuroethology of song production and perception. Since magnetic resonance imaging (MRI) represents an increasingly relevant tool for comparative neuroscience, a 3D MRI-based atlas of the starling brain becomes essential. Using multiple imaging protocols we delineated several sensory systems as well as the song control system. This starling brain atlas can easily be used to determine the stereotactic location of identified neural structures at any angle of the head. Additionally, the atlas is useful to find the optimal angle of sectioning for slice experiments, stereotactic injections and electrophysiological recordings. The starling brain atlas is freely available for the scientific community.

Keywords Songbird · European starling · High-field MRI · Brain atlas · Song control system

G. De Groof (✉) · S. Touj · E. Jonckers · A. Van der Linden
Bio-Imaging Lab, University of Antwerp, Campus Drie Eiken,
Universiteitsplein 1, 2610 Wilrijk, Belgium
e-mail: geert.degroof@uantwerp.be

I. George · S. Touj · H. Cousillas · M. Hausberger
UMR6552-Ethologie Animale Et Humaine, Université Rennes
1-CNRS, Rennes, France

M. Stacho · O. Güntürkün
Department of Biopsychology, Faculty of Psychology, Institute
of Cognitive Neuroscience, Ruhr-University Bochum,
44780 Bochum, Germany

Introduction

The European starling (*Sturnus vulgaris*) is one of the most widely used passerine species in fundamental biological research (almost 2,500 starlings were used in more than 100 studies published between 2000 and 2004; Asher and Bateson 2008). Starlings have been an important animal model in studies of ethology (e.g. Adret-Hausberger 1982; Henry et al. 1994, 2013; Hausberger et al. 1995, 1997), behavioural ecology (e.g. Powell 1974; Tinbergen 1981; Lima 1983), ecophysiology (e.g. Grue and Franson 1986; Eng et al. 2014) and neuroethology of song production and perception (Leppelsack and Vogt 1976; Hausberger and Cousillas 1995; Gentner et al. 2001; Ball and Balthazart 2001; George et al. 2004; Heimovics et al. 2011; De Groof et al. 2013; Ellis and Riters 2013).

Within the past decades, the song control system (SCS) and, to a lesser extent, the auditory systems and social behavioural network of starlings have been thoroughly examined. Up to now no atlas is available for the brain of this species, and researchers are forced to use the atlas of other songbird species like the zebra finch (Nixdorf-Bergweiler and Bischof 2007) or the canary brain (Stokes et al. 1974). Although zebra finch and canary brains are similar in size, the brain of a starling is almost three times the volume, making it hard to extrapolate stereotactic coordinates from either of the atlases to that of the starling brain. Both atlases of the songbird brain are still widely used but obviously have the limitations of all brain atlases that are based on drawings of brain sections: they not only provide a mere 2D perspective of the brain, but they are also dependent on previously specified sectioning angles.

To further neurobiological studies in starlings, we, therefore, decided to create the first 3D magnetic resonance imaging (MRI) atlas of the starling brain as a freely

available tool for the scientific community. The atlas is based on several scanning protocols, each with their own advantages and disadvantages, to visualize a wide range of neural structures. Reflecting the traditional interest in the song production and perception processes in starling, we tried to visualize the song control and auditory systems, as completely as possible. In addition we describe the different brain subdivisions as well as the main fibre tracts. We tried to establish a combined atlas that allows not only for the identification of a larger number of brain structures, but also allows researchers to select those datasets that fit best with their scientific interests. The starling brain atlas presented here can be easily adapted to match any surgical setup or histological protocol and should be appealing for future birdbrain studies. We hope that this starling brain atlas will advance studies in this songbird model in an era where traditional and MRI-based studies will intermingle more and more.

Materials and methods

Specimen preparation

For this study, one wild adult male European starling (*S. vulgaris*) caught in Normandy (France) in 2006 and kept in outdoor aviaries in Rennes (France) until the experiment, was deeply anaesthetized with pentobarbital and transcardially perfused with a phosphate-buffered heparinized saline solution (PBS, 0.12 M), followed by a mixture of paraformaldehyde (PFA, 4 %) and Dotarem® (1 %), a paramagnetic MR contrast agent. After decapitation, the head was post-fixed in a mixture of PFA (4 %) and Dotarem (1 %) for at least 5 days at 5 °C. The starling (body weight of 99.4 g) was perfused during the breeding season (25th March 2009) and the colour of its beak was yellow indicating high plasma testosterone levels (Bullough 1942; Dawson and Howe 1983; Ball and Wingfield 1987) at the time of perfusion.

Data acquisition

To obtain a 3D representation of the skull, the whole bird's head was imaged with a Siemens PET-CT equipped with a rotating 80 kV X-ray source (focal spot size of 50 µm) and a Siemens Inveon PET-CT Camera with a 125 mm X-ray detector. Isotropic voxels were acquired with a resolution of $223 \times 223 \times 223$ µm.

3D MRI datasets of the starling brain were acquired with a 9.4 T Biospec® horizontal bore NMR scanner (Bruker BioSpin, Ettlingen, Germany), equipped with a 120-mm BGA12-S actively shielded gradient-insert with a maximum gradient strength of 600 mT/m attached to an

AVANCE-II Bruker console and a 7T Pharmascan® horizontal bore NMR scanner (Bruker BioSpin, Ettlingen, Germany) equipped with a 90-mm BGA9-S actively shielded gradient-insert with a maximum gradient strength of 400 mT/m attached to an AVANCE-III Bruker console. A Bruker cross-coil setup with a linear transmit volume coil and a parallel receive surface array designed for rat head MRI was used on the 9.4T. The standard Bruker cross-coil setup with a quadrature volume coil and a quadrature surface coil for rats was used on the 7T.

Proton-density weighted 3D images were acquired on the 7T using a RARE sequence with a RARE factor of 2, a spectral bandwidth (BW) of 50 kHz, an N_{av} of 2, a TR of 500 ms and an effective TE of 25 ms. Images had a FOV of $(21.76 \times 21.76 \times 21.76)$ mm^3 with an acquisition matrix size of $(256 \times 256 \times 256)$ resulting in an isotropic spatial resolution of 85 µm in all three directions. Acquisition time was 9 h 6 min.

T2-weighted 3D images were acquired on the 9.4T using a spin echo sequence, a spectral bandwidth (BW) of 34.7 kHz, 2 averages (N_{av}), a repetition time (TR) of 5,000 ms and an echo-time (TE) of 60 ms. Images had a field of view (FOV) of $(21.76 \times 21.76 \times 21.76)$ mm^3 with an acquisition matrix size of $(256 \times 192 \times 128)$ zero-filled to $(256 \times 256 \times 256)$ resulting in an isotropic spatial resolution of 85 µm in all three directions. Acquisition time was 51 h 12 min.

T2*-weighted 3D images were acquired on the 7T using a FISP gradient echo sequence with a 15° flip-angle, a BW of 50 kHz, an N_{av} of 45, a TR of 14.31 ms, a TE of 6.5 ms and a scan repetition time of 7,500 ms. Images had a FOV of $(20.48 \times 20.48 \times 20.48)$ mm^3 with an acquisition matrix of $(512 \times 512 \times 256)$ zero-filled to $(512 \times 512 \times 512)$ resulting in an isotropic spatial resolution of 40 µm in all three directions. Acquisition time was 24 h.

Brain area delineation and 3D reconstruction

All MRI datasets and the CT dataset were co-registered with the SPM 8 package using normalized mutual information. The MRI images were used as such to co-register to each other; however, to co-register the MRI images to the CT image the brain surface was delineated from the MRI image and used as input for coregistration. The position of the ear canal and thus the most likely position of stereotactic ear-bars was established with the CT-data, and all datasets were reoriented to match a 45° angle of the ear bars and the most posterior part of the beak-opening to the horizontal axis.

All atlas delineations were performed with Amira 5.5 (Mercury Computer Systems, San Diego, CA, USA). The delineation of the skull was based on the CT dataset and was conducted automatically using a signal intensity high-

pass threshold. The brain surface and the neural subdivisions of both hemispheres were manually delineated, based on the MRI signal intensity differences between brain regions (Table 1). The delineation of each brain structure and fibre tract was performed mostly in frontal plane and subsequently controlled in the two other planes.

Results

Scanning protocols and structural delineations

Different imaging protocols provide different and complementary possibilities to delineate neural structures. *X-ray CT imaging* is essential to anchor the precise position of the brain within the skull. It thus represents a crucial first step to enable the construction of a stereotactic atlas since the brain position within the skull can be co-registered with the MR-based structural positions. We first defined a reference plane from three CT imaging based reference points: both ear canals, and the most posterior end of the beak opening. The horizontal plane of the brain atlas was then defined as a plane tilted by 45° to the reference plane about the axis running through both ear canals (Fig. 1). CT imaging is not useful to visualize brain areas. This is best done with the protocols outlined below (Table 1).

T2-weighted imaging produces images where water-containing areas become bright and fatty/cell-dense structures become dark. This sequence produced a very good anatomical image of the birdbrain with most of the brain nuclei clearly visible and delineable (Fig. 2a, b). Also the larger fibre tracts and several of the forebrain lamina could be distinguished. Although the strong signal deriving from the fluid-filled lateral ventricle made it easily detectable, this also caused a slight over-saturation, decreasing delineation accuracy of this structure. The images provided very nice contrast especially in the sagittal images. Due to zero-filling, we got more smoothed images for axial and to a lesser extent coronal images.

Proton-density weighted imaging provides images with an intermediate contrast between T1 and T2 weighted images, increasing delineation accuracy. Here we had less oversaturation of the liquid-filled lateral ventricle seen in the T2 weighted images (Fig. 2c). Since the images were obtained without zero-filling, we had very nice contrast and sharpness in all three orthogonal directions.

T2*-weighted imaging gives rise to the same type of contrast as normal T2-weighted imaging, but with much lower signal and contrast properties. However, because a gradient-echo sequence is many times faster than a spin-echo sequence, a very high resolution can be achieved within a normal time frame. Thus, at the cost of contrast, those regions that were visible could be delineated much

more accurately. Also, the high resolution of these images allowed for the detailed visualization of most of the fibre tracts (Fig. 2d). The images provide very nice contrast especially in the coronal plane. Due to zero-filling we got slightly more smoothed images for axial and sagittal images.

Although *T1 imaging* is commonly used for anatomical inspection of human brains in clinical practices, in songbird measurements this technique offers only poor regional contrast within the brain, making it rather difficult to distinguish individual brain areas from the brain's background (Vellema et al. 2011). It was, therefore, not used here.

Data presentation and validation

The co-registered MRI and CT datasets, including skull, and 46 brain subdivisions are freely available for download from our website: https://www.uantwerpen.be/en/rg/bio-imaging-lab/research/mri-atlases/starling-brain-atlas/. Data are available in Analyze format, which is supported by most 3D visualization software packages, including the free software MRIcro (http://www.cabiatl.com/mricro/mricro/mricro.html). Documentation describing how to visualize and customize the 3D datasets in MRIcro can also be found on our website.

The default data orientation is presented in a similar fashion as previously published atlases (Stokes et al. 1974; Nixdorf-Bergweiler and Bischof 2007), with a head-angle of 45°. The 45° angle has been calculated based on the axis through the ear canal (the most likely position for fixating ear bars) and the most posterior end of the beak opening relative to the horizontal plane. When loaded into MRIcro, the junction formed by the dorsocaudal cerebral vein and two branches of the transverse venous sinus (two major blood vessels running along the brain's midline), a V-shaped stereotactic landmark often used for surgical procedures, is reset to the zero-coordinate by default. This reference-point can be manually altered, however, if another zero-coordinate is preferred. In this reference frame, the X-axis represents the brain's left-to-right axis, the Y-axis corresponds to the posterior–anterior axis, and the Z-axis corresponds to the dorsal–ventral axis of the brain. The stereotactic coordinates of a specific brain area can be easily acquired by moving the cursor onto the desired region.

The 3D datasets can also be used to determine the optimal head angle for stereotactic operations or the best cutting angle for sectioning. If it is important to have multiple brain areas of interest in one single brain section, rotation and oblique slicing tools can easily be used to estimate the best cutting angle (Fig. 3).

Different datasets and delineations can be superimposed and manipulated synchronously to attain the desired brain

Table 1 Delineated structures and their systems

System	Abbreviation	Structure
Song control system	HVC	HVC
	RA	Robust nucleus of arcopallium
	X	Area X
	MMAN	Medial magnocellular nucleus of anterior nidopallium
	LMAN	Lateral magnocellular nucleus of anterior nidopallium
	DLM	Dorsolateral nucleus of medial thalamus
Auditory system	Field L	Field L
	NCM	Caudal medial nidopallium
	CMM	Caudomedial mesopallium
	Ov	Nucleus ovoidalis
	MLd	Dorsolateral nucleus of mesencephalon
Visual system	E	Entopallium
	Rt	Nucleus rotundus
	TeO	Optic tectum
Olfactory system	OB	Olfactory bulb
Social behaviour network	POM	Medial preoptic nucleus
	TnA	Nucleus taeniae amygdala
	GCt	Midbrain central grey
	LS	Lateral septum
	MS	Medial septum
	PVN	Paraventricular nucleus
	VMH	Ventromedial nucleus of the hypothalamus
	VTA	Ventral tegmental area
Fibre tracts	TSM	Septopallio-mesencephalic tract
	CoA	Anterior commissure
	CoP	Posterior commissure
	N3	Oculomotor nerve
	OM	Occipito-mesencephalic tract
	MFB	Medial forebrain bundle
	LFB	Lateral forebrain bundle
	QF	Quintofrontal tract
	FA	Fronto-arcopallial tract
	Opt	Optic tract
	DSD	Dorsal supraoptic decussation
	HiC	Hippocampal commissure
Subdivisions	N	Nidopallium
	M	Mesopallium
	A	Arcopallium
	H	Hyperpallium
	Hp	Hippocampus
	St	Striatum
	Mb	Midbrain
	Di	Diencephalon
	Cb	Cerebellum
	Pont	Pont
	LV	Lateral ventricle

Fig. 1 Overlap of MRI starling brain with delineated structures within the CT head data and the starling's brain position. The bony structure becomes more transparent from *left to right* and from *top to bottom*, giving a better view onto the brain. The *lower right* shows the brain (with subdivisions) without the skull
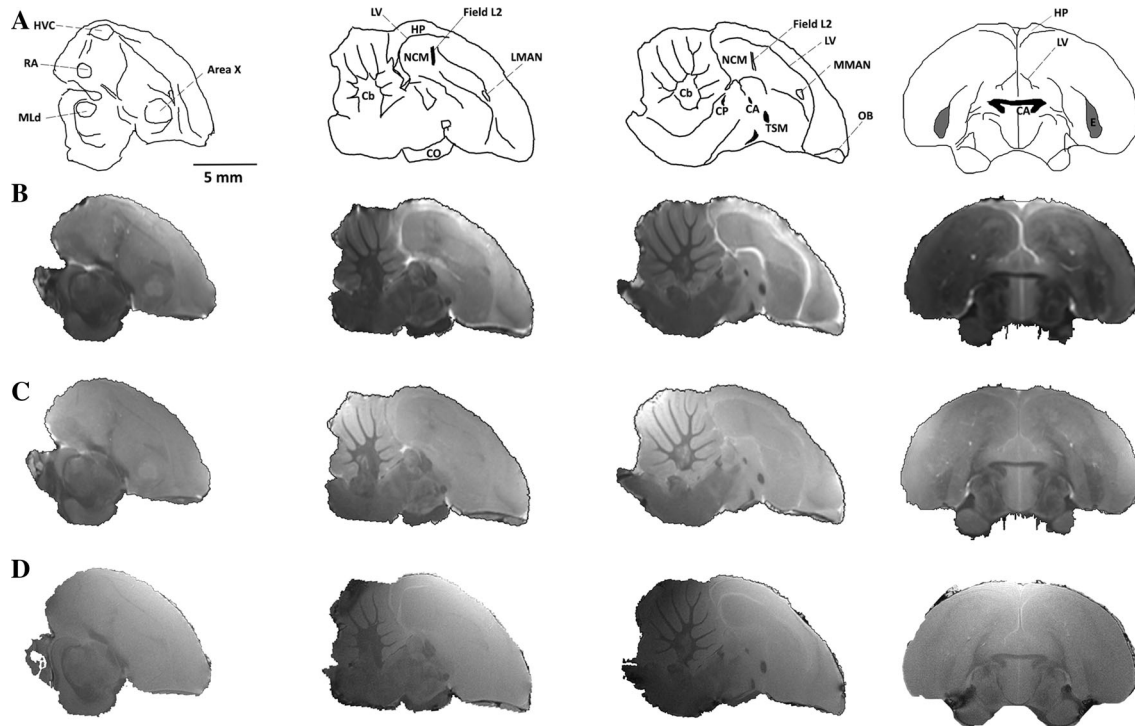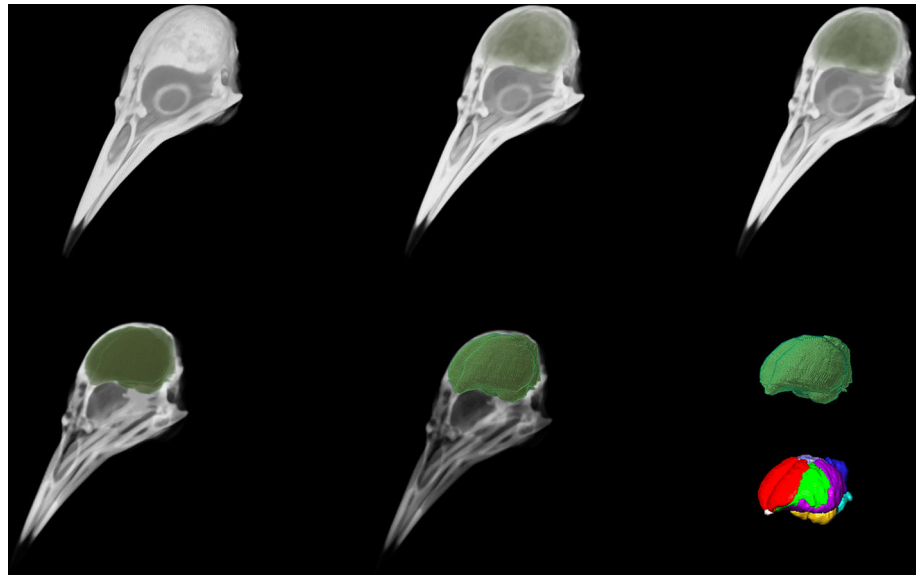
Fig. 2 Different imaging protocols offer different contrast properties. *Each row* shows three sagittal views of the starling brain at, respectively, 2.55, 1.19 and 0.60 mm from *midline* and one *axial* view at 3.50 mm anterior from the sagittal sinus bifurcation. **a** Schematic drawings illustrating important brain structures. **b** T$_2$ images show good overall anatomy, with contrasting brain nuclei. Note also the strong oversaturated signal from the lateral ventricle. **c** Proton density weighted images show good overall anatomy, with contrasting brain nuclei and less oversaturated ventricles. **d** T$_2^*$ images show a high-quality overall anatomy with distinguishable fibre tracts, at the cost of contrast in brain nuclei. *CA* anterior commissure, *Cb* cerebellum, *CP* posterior commissure, *HP* hippocampus, *HVC* used as proper name, *LV* lateral ventricle, *MLd* dorsolateral nucleus of mesencephalon, *MMAN* medial magnocellular nucleus of anterior nidopallium, *NCM* caudal medial nidopallium, *OB* olfactory bulb, *RA* robust nucleus of the arcopallium, *TSM* septopallio-mesencephalic tract
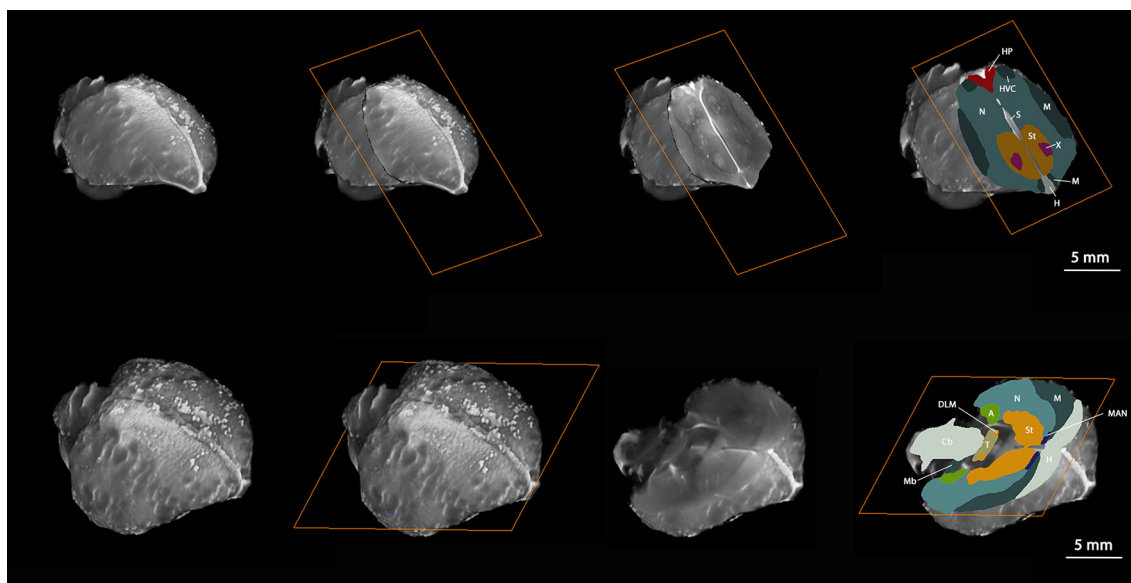
Fig. 3 Oblique slicing. 3D renderings of the brain surface showing the best cutting angle to include HVC and its efferent Area X (*top*), and DLM (dorsolateral nucleus of medial thalamus) and its efferent LMAN (*bottom* lateral magnocellular nucleus of anterior nidopallium) of both hemispheres in one sectioning plane. T₂-weighted image data are shown as raw data with overlay showing subdivisions and nuclei (*right*)

image. The delineation sets can further be used to generate a 3D representation of the brain that gives an accurate description of the relative location, shape and volume of brain areas (Figs. 4, 5).

Discussion

Because of their sophisticated vocal behaviour, their social nature, their high plasticity and their robustness, starlings have become an important model species that is widely used in the field of neuroscience (e.g. Bigalke-Kunz et al. 1987; Bee and Klump 2004; Austad 2011; Feinkohl and Klump 2011), especially in studies of neuroethology of song production and perception (e.g. Bernard et al. 1996; Bolhuis and Eda-Fujiwara 2003; Alger et al. 2009; George and Cousillas 2012; Ellis and Riters 2013). Being a seasonal species, they are also well suited for studies of neuroendocrinology and seasonal brain plasticity (e.g. Bernard and Ball 1997; Ball et al. 1999; Bentley et al. 1999; Absil et al. 2003; Alger and Riters 2006; De Groof et al. 2008, 2009, 2013; Cousillas et al. 2013).

One limitation of using starling for neuroscience research is that no detailed brain maps are available. Neurobiological scientists are forced to use 2D atlases of either the canary brain (Stokes et al. 1974) or the zebra finch brain (Nixdorf-Bergweiler and Bischof 2007) as the closest songbird brain species. However, both canary and zebra finch brains are considerably smaller than that of the starling, making it sometimes hard to find the complementary structure in the starling brain (Fig. 6). Also there might be a slight difference in relative positioning of the different nuclei between species. Traditional atlases are often based on drawings of histological brain sections and are dependent on the interests of the researcher constructing the atlas both in sectioning orientation and in delineation of brain structures. 3D imaging techniques such as MRI, however, give us the opportunity to examine the brain from a 3D, whole-brain point of view (Ma et al. 2005; Van Essen 2005; Saleem and Logothetis 2007; Poirier et al. 2008; Datta et al. 2012; Muñoz-Moreno et al. 2013; Güntürkün et al. 2013; Nie et al. 2013; Kumazawa-Manita et al. 2013; Ullmann et al. 2014). Here we present the first 3D MRI-based atlas of the starling brain, a model system often used for neurobiological and behavioural studies. We tried to capture as many different brain regions as possible, making this atlas suitable for many different fields of birdbrain research. There are several advantages in the brain atlas that we present here over the previously published 2D atlas of the canary brain (Stokes et al. 1974) and similar brain atlases of other bird species (e.g. Karten and Hodos 1967; Nixdorf-Bergweiler and Bischof 2007; Puelles et al. 2007). First and foremost, the 3D capturing methods used in this study allowed us to study the anatomy of a single brain from any possible angle, eliminating the limitations of 2D atlases that are inherently restricted to a specified orientation.

This approach is particularly useful in combination with other whole-brain imaging techniques such as functional MRI (Van Meir et al. 2005; Voss et al. 2007; Poirier et al.
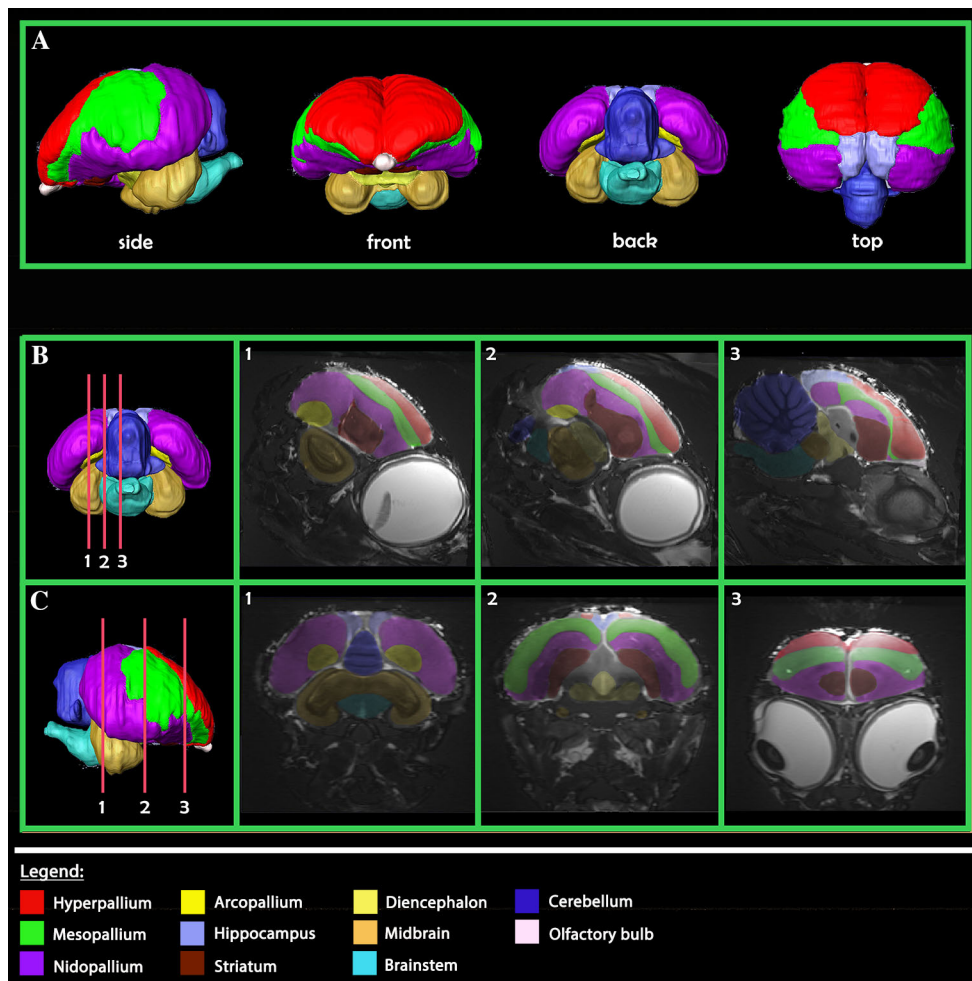
Fig. 4 **a** 3D rendering of the brain with subdivisions. **b** Transparent overlay showing the brain (T_2 weighted image) with delineated subdivisions on sagittal slices. **c** Transparent overlay showing the brain (T_2 weighted image) with delineated subdivisions on axial slices

Fig. 5 3D rendering of the brain. **a** Non-transparent rendering showing the outer brain surface with delineated subdivisions. **b** Transparent rendering showing the brain nuclei
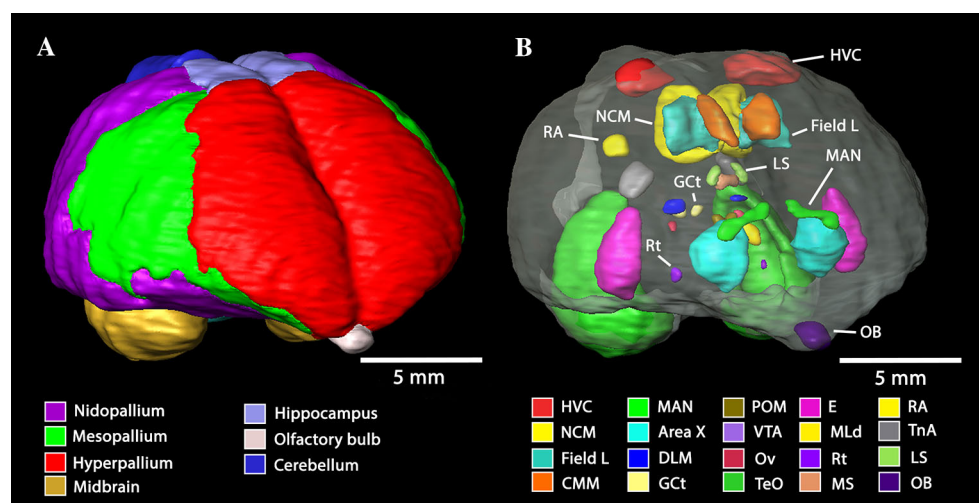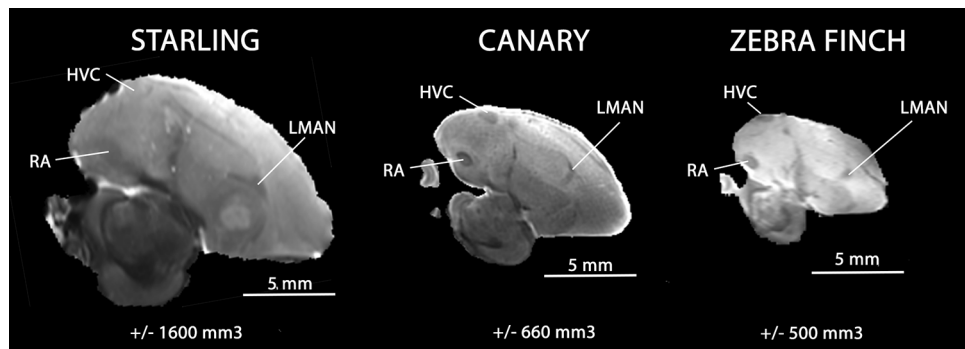
Fig. 6 Para-sagittal MRI slice through HVC, *RA* (robust nucleus of arcopallium) and *LMAN* (lateral magnocellular nucleus of anterior nidopallium) in three different songbird species. MRI images are all T_2 weighted. Canary data are from (Vellema et al. 2011) and zebra finch data are from (Poirier et al. 2008). The approximate volume of the brain per species is indicated below each slice

2009; De Groof et al. 2013; Van Ruijssevelt et al. 2013) and Diffusion Tensor Imaging (De Groof et al. 2009). The atlas could be applied as a template for (future) studies of these types in starlings (De Groof et al. 2013).

The possibility to reset the coordinate system of the brain-model to any preferred orientation makes it customizable to any stereotactic device that may be used for brain injections or electrophysiological recordings. Besides locating target areas based on stereotactic coordinates, the 3D brain atlas is well suited to optimize surgical protocols to avoid damage in specified regions. When injecting a tract-tracer in RA for example (e.g. Kirn et al. 1999; Roberts et al. 2008), the brain atlas could be used to calculate the optimal head angle to avoid any leakage from the injection tract into its afferent nucleus HVC, which is located directly above RA at certain angles. Alternatively, one might want to angle the head to the side to avoid puncturing the lateral ventricle, which could lead to an unwanted spread of a chemical through the brain.

The reorientation possibilities of the atlas are also well suited to calculate the best angle for making brain sections that contain multiple regions of interest (Fig. 3). This could be very useful for histological staining procedures or in situ hybridization protocols (e.g. Jarvis and Nottebohm 1997; Tramontin et al. 1998; Metzdorf et al. 1999) in which two or more brain areas are requested in a single brain section, potentially making comparative quantification studies more reliable and less time consuming.

For electrophysiological recordings in brain slices (Mooney and Prather 2005; Gale and Perkel 2006; Meitzen et al. 2009) it can be useful to calculate the ideal sectioning angles, not only to include two targets of interest, but also to include intact fibre tracts running between the two regions within one recording slice. The same is true for high-density multi-electrode recordings (Amin et al. 2013; Cousillas et al. 2013), where the final measurement sites

are highly dependent on the insertion angle of the electrode array.

Finally, because the brain atlas has been constructed with the skull intact, without the need for dehydration or freeze-protection steps, the shape of the brain will be relatively close to the in vivo situation. In contrast, 2D atlases that are based on histological sections have to deal with inaccuracies that are introduced during the histological procedures (Ma et al. 2005; Vellema et al. 2011). Dehydration steps that are often necessary for histological preparations cause a severe shrinkage of the brain, and additional shape-artefacts are virtually unavoidable during the cutting and mounting process.

As with 2D histological atlases, this 3D MRI brain atlas is based on one individual's data, in this case a male starling during the breeding season. This is important because of both sexual dimorphisms and seasonal differences in brain nuclei size. One should, therefore, be cautious when attempting to obtain coordinates for certain nuclei of female starling studies (although starlings show less sexual dimorphism than, e.g. the zebra finch; Bernard et al. 1993; Ball et al. 1994) or non-breeding season male starlings. Regions known to be variable in size according to season are most of the song control nuclei (e.g. HVC, RA and Area X) (Ball and Bentley 2000; Tramontin and Brenowitz 2000), nuclei of the social behaviour network (e.g. POM Riters et al. 2000) and NCM (De Groof et al. 2009).

The 3D starling brain atlas presented here could be used as a framework for researchers working on the starling brain, and for avian brain research in general. Together with our previously published 3D brain atlases of the zebra finch (Poirier et al. 2008), of the canary (Vellema et al. 2011) and of a non-songbird species (e.g. the pigeon brain (Güntürkün et al. 2013)), we now have four detailed, easily adaptable brain atlases for four commonly studied species of birds that should appeal to scientists from different

disciplines working on the function, physiology and anatomy of the avian brain.

Ethical standard All applicable international, national, and/or institutional guidelines for the care and use of animals were followed. All procedures performed in studies involving animals were in accordance with the ethical standards of the institution or practice at which the studies were conducted.

References

Absil P, Pinxten R, Balthazart J, Eens M (2003) Effect of age and testosterone on autumnal neurogenesis in male European starlings (*Sturnus vulgaris*). Behav Brain Res 143:15–30. doi:10.1016/s0166-4328(03)00006-8

Adret-Hausberger M (1982) Social influences on the whistled songs of starlings. Behav Ecol Sociobiol 11:241–246

Alger SJ, Riters LV (2006) Lesions to the medial preoptic nucleus differentially affect singing and nest box-directed behaviors within and outside of the breeding season in European starlings (*Sturnus vulgaris*). Behav Neurosci 120:1326–1336

Alger SJ, Maasch SN, Riters LV (2009) Lesions to the medial preoptic nucleus affect immediate early gene immunolabeling in brain regions involved in song control and social behavior in male European starlings. Eur J Neurosci 29:970–982. doi:10.1111/j.1460-9568.2009.06637.x

Amin N, Gastpar M, Theunissen FE (2013) Selective and efficient neural coding of communication signals depends on early acoustic and social environment. PLoS One 8:e61417. doi:10.1371/journal.pone.0061417

Asher L, Bateson M (2008) Use and husbandry of captive European starlings (*Sturnus vulgaris*) in scientific research: a review of current practice. Lab Anim 42:111–126. doi:10.1258/la.2007.007006

Austad SN (2011) Candidate bird species for use in aging research. ILAR J 52:89–96

Ball GF, Balthazart J (2001) Ethological concepts revisited: immediate early gene induction in response to sexual stimuli in birds. Brain Behav Evol 57:252–270. doi:10.1159/000047244

Ball GF, Bentley GE (2000) Neuroendocrine mechanisms mediating the photoperiodic and social regulation of seasonal reproduction in birds. In: Wallen K, Schneider F (eds) Reproduction in context. MIT Press, Cambridge, MA, pp 129–158

Ball GF, Wingfield JC (1987) Changes in plasma levels of sex steroids in relation to multiple broodedness and nest site density in male starlings. Physiol Zool 60:191–196

Ball GF, Casto JM, Bernard DJ (1994) Sex-differences in the volume of avian song control nuclei—comparative-studies and the issue

of brain nucleus delineation. Psychoneuroendocrinology 19:485–504

Ball GF, Bernard DJ, Foidart A et al (1999) Steroid sensitive sites in the avian brain: does the distribution of the estrogen receptor alpha and beta types provide insight into their function? Brain Behav Evol 54:28–40

Bee MA, Klump GM (2004) Primitive auditory stream segregation: a neurophysiological study in the songbird forebrain. J Neurophysiol 92:1088–1104. doi:10.1152/jn.00884.2003

Bentley GE, Van't Hof TJ, Ball GF (1999) Seasonal neuroplasticity in the songbird telencephalon: a role for melatonin. Proc Natl Acad Sci USA 96:4674–4679

Bernard DJ, Ball GF (1997) Photoperiodic condition modulates the effects of testosterone on song control nuclei volumes in male European starlings. Gen Comp Endocrinol 105:276–283

Bernard DJ, Casto JM, Ball GF (1993) Sexual dimorphism in the volume of song control nuclei in European starlings: assessment by a Nissl stain and autoradiography for muscarinic cholinergic receptors. J Comp Neurol 334:559–570. doi:10.1002/cne.903340405

Bernard DJ, Eens M, Ball GF (1996) Age- and behavior-related variation in volumes of song control nuclei in male European starlings. J Neurobiol 30:329–339. doi:10.1002/(SICI)1097-4695(199607)30:3<329:AID-NEU2>3.0.CO;2-6

Bigalke-Kunz B, Rübsamen R, Dörrscheidt GJ (1987) Tonotopic organization and functional characterization of the auditory thalamus in a songbird, the European starling. J Comp Physiol A 161:255–265. doi:10.1007/BF00615245

Bolhuis JJ, Eda-Fujiwara H (2003) Bird brains and songs: neural mechanisms of birdsong perception and memory. Anim Biol 53:129–145. doi:10.1163/157075603769700331

Bullough WS (1942) The reproductive cycles of the British and continental races of the starling (*Sturnus vulgaris* L.). Phil trans R Soc Lond B 231:165–246

Cousillas HH, George II, Alcaix SS et al (2013) Seasonal female brain plasticity in processing social vs. sexual vocal signals. Eur J Neurosci 37:728–734. doi:10.1111/ejn.12089

Datta R, Lee J, Duda J et al (2012) A digital atlas of the dog brain. PLoS One 7:e52140. doi:10.1371/journal.pone.0052140

Dawson A, Howe PD (1983) Plasma corticosterone in wild starlings (*Sturnus vulgaris*) immediately following capture and in relation to body weight during the annual cycle. Gen Comp Endocrinol 51:303–308

De Groof G, Verhoye M, Van Meir V et al (2008) Seasonal rewiring of the songbird brain: an in vivo MRI study. Eur J Neurosci 28:2475–2485. doi:10.1111/j.1460-9568.2008.06545.x (discussion 2474)

De Groof G, Verhoye M, Poirier C et al (2009) Structural changes between seasons in the songbird auditory forebrain. J Neurosci 29:13557–13565. doi:10.1523/JNEUROSCI.1788-09.2009

De Groof G, Poirier C, George I et al (2013) Functional changes between seasons in the male songbird auditory forebrain. Front Behav Neurosci 7:196. doi:10.3389/fnbeh.2013.00196

Ellis JMS, Riters LV (2013) Patterns of FOS protein induction in singing female starlings. Behav Brain Res 237:148–156. doi:10.1016/j.bbr.2012.09.004

Eng ML, Williams TD, Letcher RJ, Elliott JE (2014) Assessment of concentrations and effects of organohalogen contaminants in a terrestrial passerine, the European starling. Sci Total Environ 473:589–596. doi:10.1016/j.scitotenv.2013.12.072

Feinkohl A, Klump G (2011) Processing of transient signals in the visual system of the European starling (*Sturnus vulgaris*) and humans. Vis Res 51:21–25. doi:10.1016/j.visres.2010.09.020

Gale SD, Perkel DJ (2006) Physiological properties of zebra finch ventral tegmental area and substantia nigra pars compacta neurons. J Neurophysiol 96:2295–2306. doi:10.1152/jn.01040.2005

Gentner TQ, Hulse SH, Duffy D, Ball GF (2001) Response biases in auditory forebrain regions of female songbirds following exposure to sexually relevant variation in male song. J Neurobiol 46:48–58

George I, Cousillas H (2012) How social experience shapes song representation in the brain of starlings. J Physiol Paris. doi:10.1016/j.jphysparis.2012.12.002

George I, Vernier B, Richard JP et al (2004) Hemispheric specialization in the primary auditory area of awake and anesthetized starlings (*Sturnus vulgaris*). Behav Neurosci 118:597–610. doi:10.1037/0735-7044.118.3.597

Grue CE, Franson LP (1986) Use of captive starlings to determine effects of environmental contaminants on passerine reproduction—pen characteristics and nestling food-requirements. Bull Environ Contam Toxicol 37:655–663

Güntürkün O, Verhoye M, De Groof G, Van der Linden A (2013) A 3-dimensional digital atlas of the ascending sensory and the descending motor systems in the pigeon brain. Brain Struct Funct 218:269–281. doi:10.1007/s00429-012-0400-y

Hausberger M, Cousillas H (1995) Categorization in birdsong: from behavioural to neuronal responses. Behav Process 35:83–91

Hausberger M, Richard-Yris MA, Henry L et al (1995) Song sharing reflects the social organization in a captive group of European starlings (Sturnus vulgaris). J Comp Psychol 109:222–241

Hausberger M, Forasté MA, Richard-Yris CN (1997) Differential response of female starlings to shared and nonshared song types. Etologia 5:31–38

Heimovics SA, Cornil CA, Ellis JMS et al (2011) Seasonal and individual variation in singing behavior correlates with alpha 2-noradrenergic receptor density in brain regions implicated in song, sexual, and social behavior. Neuroscience 182:133–143. doi:10.1016/j.neuroscience.2011.03.012

Henry L, Hausberger M, Jenkins PF (1994) The use of song repertoire changes with pairing status in male European starling. Bioacoustics 5:261–266

Henry L, Bourguet C, Coulon M et al (2013) Sharing mates and nest boxes is associated with female "friendship" in European starlings, Sturnus vulgaris. J Comp Psychol 127:1–13. doi:10.1037/a0029975

Jarvis ED, Nottebohm F (1997) Motor-driven gene expression. Proc Natl Acad Sci USA 94:4097–4102

Karten HJ, Hodos W (1967) A stereotaxic atlas of the brain of the pigeon. Johns Hopkins Press, Baltimore

Kirn JR, Fishman Y, Sasportas K et al (1999) Fate of new neurons in adult canary high vocal center during the first 30 days after their formation. J Comp Neurol 411:487–494. doi:10.1002/(SICI)1096-9861(19990830)411:3<487:AID-CNE10>3.0.CO;2-M

Kumazawa-Manita N, Katayama M, Hashikawa T, Iriki A (2013) Three-dimensional reconstruction of brain structures of the rodent Octodon degus: a brain atlas constructed by combining histological and magnetic resonance images. Exp Brain Res Exp Hirnforsch Exp Cereb 231:65–74. doi:10.1007/s00221-013-3667-1

Leppelsack HJ, Vogt M (1976) Responses of auditory neurons in forebrain of a songbird to stimulation with species-specific sounds. J Comp Physiol 107:263–274

Lima SL (1983) Patch sampling behavior of starlings foraging in simple patchy environments. Am Zool 23:897

Ma Y, Hof PR, Grant SC et al (2005) A three-dimensional digital atlas database of the adult C57BL/6J mouse brain by magnetic resonance microscopy. Neuroscience 135:1203–1215. doi:10.1016/j.neuroscience.2005.07.014

Meitzen J, Weaver AL, Brenowitz EA, Perkel DJ (2009) Plastic and stable electrophysiological properties of adult avian forebrain song-control neurons across changing breeding conditions.

J Neurosci 29:6558–6567. doi:10.1523/JNEUROSCI.5571-08.2009

Metzdorf R, Gahr M, Fusani L (1999) Distribution of aromatase, estrogen receptor, and androgen receptor mRNA in the forebrain of songbirds and nonsongbirds. J Comp Neurol 407:115–129

Mooney R, Prather JF (2005) The HVC microcircuit: the synaptic basis for interactions between song motor and vocal plasticity pathways. J Neurosci 25:1952–1964. doi:10.1523/JNEUROSCI.3726-04.2005

Muñoz-Moreno E, Arbat-Plana A, Batalle D et al (2013) A magnetic resonance image based atlas of the rabbit brain for automatic parcellation. PLoS One 8:e67418. doi:10.1371/journal.pone.0067418

Nie B, Chen K, Zhao S et al (2013) A rat brain MRI template with digital stereotaxic atlas of fine anatomical delineations in paxinos space and its automated application in voxel-wise analysis. Hum Brain Mapp 34:1306–1318. doi:10.1002/hbm.21511

Nixdorf-Bergweiler BE, Bischof HJ (2007) A stereotaxic atlas of the brain of the zebra finch Taeniopygia guttata with special emphasis on telencephalic visual and song system nuclei in transverse and sagittal sections. National Library of Medicine, Bethesda

Poirier C, Vellema M, Verhoye M et al (2008) A three-dimensional MRI atlas of the zebra finch brain in stereotaxic coordinates. Neuroimage 41:1–6. doi:10.1016/j.neuroimage.2008.01.069

Poirier C, Boumans T, Verhoye M et al (2009) Own-song recognition in the songbird auditory pathway: selectivity and lateralization. J Neurosci 29:2252–2258. doi:10.1523/JNEUROSCI.4650-08.2009

Powell G (1974) Experimental analysis of social value of flocking by starlings (Sturnus vulgaris) in relation to predation and foraging. Anim Behav 22:501–505. doi:10.1016/S0003-3472(74)80049-7

Puelles L, Martinez-de-la-Torre M, Paxinos G et al (2007) The chick brain in stereotaxic coordinates: an atlas featuring neurometric subdivisions and mammalian homologies. Academic Press, San Diego

Riters LV, Eens M, Pinxten R et al (2000) Seasonal changes in courtship song and the medial preoptic area in male European starlings (Sturnus vulgaris). Horm Behav 38:250–261

Roberts TF, Klein ME, Kubke MF et al (2008) Telencephalic neurons monosynaptically link brainstem and forebrain premotor networks necessary for song. J Neurosci 28:3479–3489. doi:10.1523/JNEUROSCI.0177-08.2008

Saleem KS, Logothetis NK (2007) A combined MRI and histology atlas of the rhesus monkey brain in stereotaxic coordinates. Academic Press, San Diego

Stokes TM, Leonard CM, Nottebohm F (1974) The telencephalon, diencephalon, and mesencephalon of the canary, Serinus canaria, in stereotaxic coordinates. J Comp Neurol 156:337–374

Tinbergen JM (1981) Foraging decisions in starlings (Sturnus vulgaris L). Ardea 69:1–67

Tramontin AD, Brenowitz EA (2000) Seasonal plasticity in the adult brain. Trends Neurosci 23:251–258

Tramontin AD, Smith GT, Breuner CW, Brenowitz EA (1998) Seasonal plasticity and sexual dimorphism in the avian song control system: stereological measurement of neuron density and number. J Comp Neurol 396:186–192

Ullmann JFP, Watson C, Janke AL et al (2014) An MRI atlas of the mouse basal ganglia. Brain Struct Funct 219:1343–1353. doi:10.1007/s00429-013-0572-0

Van Essen DC (2005) A population-average, landmark- and surface-based (PALS) atlas of human cerebral cortex. Neuroimage 28:635–662. doi:10.1016/j.neuroimage.2005.06.058

Van Meir V, Boumans T, De Groof G et al (2005) Spatiotemporal properties of the BOLD response in the songbirds' auditory

circuit during a variety of listening tasks. Neuroimage 25:1242–1255. doi:10.1016/j.neuroimage.2004.12.058

Van Ruijssevelt L, De Groof G, Van der Kant A et al (2013) Functional magnetic resonance imaging (FMRI) with auditory stimulation in songbirds. J Vis Exp. doi:10.3791/4369

Vellema M, Verschueren J, Van Meir V, Van der Linden A (2011) A customizable 3-dimensional digital atlas of the canary brain in

multiple modalities. Neuroimage 57:352–361. doi:10.1016/j. neuroimage.2011.04.033

Voss HU, Tabelow K, Polzehl J et al (2007) Functional MRI of the zebra finch brain during song stimulation suggests a lateralized response topography. Proc Natl Acad Sci USA 104:10667–10672